Korean J. Chem. Eng., 40(9), 2356-2364 (2023)
DOI: 10.1007/s11814-023-1468-1

pISSN: 0256-1115
eISSN: 1975-7220

Synthesis and characterization of epoxy resin-based ion-imprinted polymer for selective removal of copper ions

Sining Zhu, Haitao Wan, Zhibo Yan, Chen Xi, Yuzhuo Zhang, and Fan Zhang†

College of Chemistry and Chemical Engineering, National Experimental Teaching Demonstration Center for Chemistry, Jishou University, Jishou 416000, China
(*Received 28 November 2022 • Revised 3 April 2023 • Accepted 7 April 2023*)

Abstract−With the continuous development of the concept of green chemistry, more attention is being paid to the selective capture of copper (II) from wastewater and its recovery and reuse. Ion imprinting technology is widely used to remove heavy metals from aqueous solutions due to its high selectivity. In this work, Cu(II) imprinted polymer (Cu(II)-IIP) was prepared by stepwise polymerization using Cu(II) ions as the template ions, PEG-600 as a pore-forming agent, epoxy resin as the carrier, and polyethylene polyamine as curing agent and complexing agent. The influences of solution pH, reaction temperature, reaction time and initial solubility of metal ions on its adsorption ability were systematically examined. The studies showed that the maximum adsorption quantity was 91.58 mg/g when pH=5 and T=318 K. The adsorption for Cu(II) of the Cu(II)-IIP was considered to be the monolayer chemisorption and spontaneous endothermic process. In the presence of multiple coexisting ions, Cu(II)-IIP had high selectivity for Cu(II). After five adsorption-desorption cycles, high removal rate could still be obtained, which means that the material provides a feasible method for treating wastewater containing Cu(II) ions.

Keywords: Cu(II) Ions, Ion-imprinted Polymer, Adsorption, Epoxy Resin, Heavy Metal

INTRODUCTION

In recent years, with rapid industrial development, heavy metal pollution has become more and more serious. In addition to being toxic and difficult to degrade, heavy metal wastewater can also be transformed into more toxic organic compounds in living organisms through a series of complex effects. Consequently, there is a serious risk to both human health and the ecological environment [1,2]. For example, mercury, cadmium, lead, copper and arsenic are several common metals in wastewater that are widely sourced from smelting, electroplating, chemical industry, non-ferrous metal mining, electronic material rinsing wastewater, dye production and other processes [3-5]. Cu(II) ion is a trace element in the body that is involved in a variety of physiological processes; however, excessive copper intake can cause a variety of problems, such as headaches, vomiting, nausea, liver and kidney failure [6]. Therefore, the search for a way to take Cu(II) ions out of the environment has become the direction of concern. Currently, the treatment methods for Cu(II) ions wastewater at domestic and foreign mainly include adsorption, ion exchange, electrochemical, and membrane separation methods [7-10]. Among them, the adsorption method has gotten more and more attention because of its several advantages including flexible design, efficiency in dealing with water pollution and adsorbent regeneration [11]. As the core of the adsorption method, the adsorbents can be classified into natural, biological and synthetic adsorbents according to the source and chemical structure [12]. Among them, synthetic adsorbents have a certain development potential in the field of modern adsorption technology due to their high adsorption capacity. Among the synthetic adsorbents, ion-imprinted polymers (IIPs) are described as the "ionic key" to contemporary manufacturing identification. The IIPs can selectively identify and adsorb template ions in specific environments, resulting in the characteristics of high selectivity and easy regeneration [13,14].

For excellent IIP materials, the selection of suitable carriers can effectively improve the recognition selectivity of the ion-imprinted materials for the template ions [15,16]. The main carriers for constructing Cu(II) ion imprinting materials include 2′-bipyridine and 4-vinyl pyridine [17], acrylic acid-modified polyethersulfone membrane [18], 2-mercaptobenzimidazole [19], 4-aminophenol-indigo Schiff base [20], and chitosan [21]. However, the preparation process of these imprinted materials is more complicated and the preparation cost is higher. Therefore, the research for non-toxic and inexpensive carriers is one of the keys of ion imprinting materials from laboratory to practical application and industrialization. Bisphenol A epoxy resin based on its low cost, good thermosetting properties and chemical stability makes it consistent with the concept of green chemistry development and has good prospects for development. At present, the choice of epoxy resin as the carrier for imprinting and combining it with ion imprinting technology is an innovation. Wang et al. prepared a polymer monolithic stir-bar from epoxy resin, which not only has good adsorption effect but also greatly improves the recovery rate and reusable times [22,23]. However, due to some difficulties in the preparation of large-scale monolithic stir-bars, there are few applications in the industrial field. In addition, although some studies have been conducted on the prepa-

†To whom correspondence should be addressed.
E-mail: chemfzhang@163.com

ration of imprinted adsorbents, the cross-linking of Cu(II) imprinted epoxy resin with polyethylene polyamines has not been found by consulting the recent literature.

In this work, epoxy resin-based Cu(II) imprinted polymer was proposed to be prepared by stepwise polymerization employing Cu(II) ions as the template ions, bisphenol A epoxy resin (BPA-EP) acting as the carrier, and polyethylene polyamines as the curing agent and complexing agent, the samples were characterized and analyzed by SEM, FT-IR, XPS and TGA techniques, and their surface composition and adsorption mechanism were further analyzed.

MATERIALS AND METHODS

1. Materials and Reagents

Polyethylene polyamine (PEPA) was purchased from Aladdin (Shanghai, China). BPA-EP was provided from Baling Petrochemical Co., Ltd, (Yueyang, China). Copper nitrate [$Cu(NO_3)_2{\cdot}3H_2O$] was purchased from Kemiou (Tianjin, China). Polyethylene glycol (PEG-600) was purchased from Kemiou (Tianjin, China). Ethylenediaminetetraacetic acid disodium salt (EDTA) was purchased from Sinopharm Chemical Reagent Co., Ltd, (Sinopharm, China). Methyl alcohol (CH_3OH) was purchased from Fuyu Chemical Reagent Co., Ltd, (Tianjin, China). Sodium hydroxide (NaOH), acetone (CH_3COCH_3) and nitric acid (HNO_3) were purchased from Jinshan Chemical Reagent Co., Ltd, (Chengdu, China). The chemical reagents employed in the investigation were analytical grade, and all solutions were made using distilled water.

2. Preparation of Cu(II)-IIP and Cu(II)-NIP

Cu(II)-IIP and Cu(II)-NIP were created using stepwise polymerization [24]. First, 0.74 g of $Cu(NO_3)_2{\cdot}3H_2O$ was dissolved in 15.6 g of PEG-600 and stirred well until completely dissolved. Subsequently, 13.2 g of BPA-EP and 9.8 g of PEPA were added and stirred thoroughly, then the material was placed in an ultrasonic shaker at 60 °C for 10 min to make PEG-600 evenly dispersed, and then sealed in an oven at 60 °C for 12 h. The obtained solid was crushed to 70-90 μm with a high-speed crusher and rinsed three times with distilled water at 60 °C for 2 hours each time to remove PEG-600, and eluted with 0.1 mol/L EDTA solution at 40 °C with ultrasound until there were no Cu(II) ions in the solution. Then, they were neutrally washed with distilled water before being dried in a constant temperature oven at 60 °C for 24 hours and set aside. The non-imprinted polymer (Cu(II)-NIP) was prepared under conditions without the addition of Cu(II) as the imprinted template ions, and all other experimental steps were the same as the preparation of Cu(II)-IIP. Fig. 1 depicts the synthetic mechanism of Cu(II)-IIP based on BPA-EP.

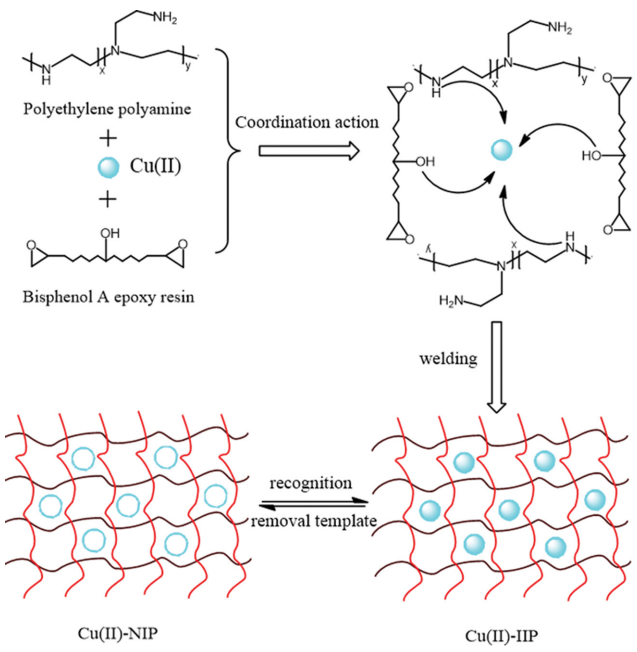

Fig. 1. The synthetic mechanism of the Cu(II)-IIP based on BPA-EP.

3. Instrumentation and Characterization

An atomic absorption spectrometer (AA-6300C, Shimadzu, Japan) was used to determine the Cu(II) concentration before and after adsorption. The chemical composition and functional group changes on the sample surface were investigated by the KBr compression method using Fourier transform infrared spectroscopy (Nicolet IS10, Kulite, USA). The surface morphology and element analysis of Cu(II)-IIP were studied using scanning electron microscopy and energy dispersive spectroscopy (Nova NanoSEM 450, FEI, USA). The thermal stability of dried Cu(II)-IIP samples before and after adsorption was determined using a thermogravimetric analyzer (TGA-DSC, Mettler Toledo, USA) in the 25-800 °C temperature range (10 °C/min). The adsorbents were analyzed by X-ray photoelectron spectroscopy (ESCALAB Xi+, Thermo Fisher, UK) to determine the composition of the adsorbent.

4. Batch Adsorption Experiments

The specific experimental procedure is as follows: The Cu(II) ions stock solution of the required concentration for the experiment was made using appropriate amounts of $Cu(NO_3)_2{\cdot}3H_2O$ and distilled water. The effects of pH on the experiments were investigated as follows: the 0.1 mol/L HNO_3 or 0.1 mol/L NaOH solution was slowly added to make the pH range 3.0-6.0, and static adsorption was performed at a temperature of 298 K and a concentration of 100 mg/L for 12 h. The initial concentration range of solution was changed from 20 to 100 mg/L, and the impact of the initial concentration of metal ions on the experiments was investigated at an initial temperature of 298 K and an optimal pH value. Under the condition of optimum pH value and an initial temperature of 298 K, the solution of 100 mg/L was prepared and the adsorption kinetics experiments were performed within 420 min. The adsorption isotherm experiments were studied at three temperatures of 298, 308 and 318 K by configuring solutions with initial concentrations of 20 to 120 mg/L, respectively. During the batch adsorption tests, 50 mL of the desired Cu(II) solution concentration was combined thoroughly with 50 mg of adsorbent in conical flasks, the flask was sealed with plastic wrap and placed in a water-bath thermostatic shaker with a stirring rate of 120 r/min. After adsorption, the supernatant was filtered, and the remaining metal ion concentration in the filtrate was determined and calculated using the FAAS method to determine the adsorption capacity [25].

Results using the average values of three groups of parallel tests, the adsorption capacity (Q_e, Q_t, $mg{\cdot}g^{-1}$) and removal rate (R, %) of metal ions were determined using Eqs. (1), (2) and (3) [26,27]:

$$Q_t = \frac{(C_0 - C_t)V}{W} \quad (1)$$

$$Q_e = \frac{(C_0 - C_e)V}{W} \quad (2)$$

$$R = \frac{C_0 - C_e}{C_0} \times 100\% \quad (3)$$

where C_0, C_e and C_t (mg/L) are the initial, equilibrium and time t concentrations of Cu(II) ions, V (L) is the volume of the solution and W (g) is the mass of the adsorbent, t_e (min) is the time to reach adsorption equilibrium, Q_e and Q_t (mg·g^{-1}) are the adsorption capacities at t_e and t, respectively.

5. Selectivity Experiments

The selectivity of Cu(II)-IIP and Cu(II)-NIP for Cu(II) ions was evaluated using batch multiplex competitive adsorption experiments (n=3). 50 mg of the adsorbents was added to 50 mL of a solution containing 100 mg/L of Cd(II), Mn(II), Zn(II), and Cu(II) ions at 298 K and optimum pH and shaken at constant temperature for 5 h.

In this experiment, imprinting factor α and selection factor β were used to assess the selective adsorption capacity of the materials, which were obtained from Eqs. (4) and (5), respectively [28,29]:

$$\alpha = \frac{Q_{eCu(II)\text{-}IIP}}{Q_{eCu(II)\text{-}NIP}} \quad (4)$$

$$\beta = \frac{\alpha_t}{\alpha_c} \quad (5)$$

where $Q_{eCu(II)\text{-}IIP}$ and $Q_{eCu(II)\text{-}NIP}$ (mg·g^{-1}) represent the adsorption amounts of Cu(II)-IIP and Cu(II)-NIP on template ions, respectively, α_t and α_c represent the imprinting factors of Cu(II)-IIP on template ions and competing ions, respectively.

6. Reusability Experiments

The Cu(II) solution with a concentration of 40 mg/L and the adsorbents were subjected to static adsorption for 5 h at 298 K and optimal pH value. After adsorption, the supernatant was filtered and the concentration of remaining Cu(II) ions was determined. The adsorbents were fully washed with 0.1 mol/L EDTA for 6 h to remove Cu(II) ions and then washed with distilled water until the pH of the solution was neutral. The adsorbents were used for the subsequent experiment, the above operation being repeated, and five cycles of adsorption-desorption studies were carried out.

RESULTS AND DISCUSSION

1. Characterization

1-1. FT-IR Analysis and Thermogravimetric Analysis

The FT-IR spectra of Cu(II)-IIP before and after the adsorption of Cu(II) are shown in Fig. 2(a); a and b are the curves before and after the adsorption, respectively. The vibrational absorption peaks corresponding to the epoxy group were not found in the figure, indicating that the epoxy group underwent a ring opening reaction [22]. It is easily found that the absorption peaks at 3,424 cm^{-1} and 1,630 cm^{-1} were due to the deformation vibration of O-H, and N-H from the curve a. These vibrational absorption peaks indicate the successful substitution of the epoxy group in the epoxy resin and verify the effective cross-linking process of Cu(II)-IIP [30,31]. The absorption peak of Cu(II)-IIP at 1,250 cm^{-1} was caused by the vibration of the C-O-C stretching on epoxy resin [32]. After the adsorption, the absorption peaks were moved from 1,630 cm^{-1} to 1,617 cm^{-1} and increasing the peaks intensity, which indicates that Cu(II) underwent strong coordination with the amino group in the adsorption process and Cu(II) joined with Cu(II)-IIP to create a complex [33].

Fig. 2(b) shows the thermal weight loss curves before and after adsorption of the Cu(II)-IIP on Cu(II) under nitrogen atmosphere. The small weight loss of Cu(II)-IIP before and after adsorption at 90-117 °C was attributed to the evaporation of residual water in Cu(II)-IIP, the weight loss at 117-296 °C was credited with the decomposition of amino and oxygen-containing functional groups, and the rapid weight loss at 300-410 °C was attributed to the decomposition and carbonization of the polymer carbon skeleton [16]. The percentage mass of the remaining sample after adsorption was higher than that before adsorption because Cu(II) underwent oxidative conversion to CuO that could not be decomposed during the heating process [26].

1-2. SEM and EDS Analysis of the Cu(II)-IIP

Fig. 3(a), (b) shows the surface morphology of Cu(II)-IIP before

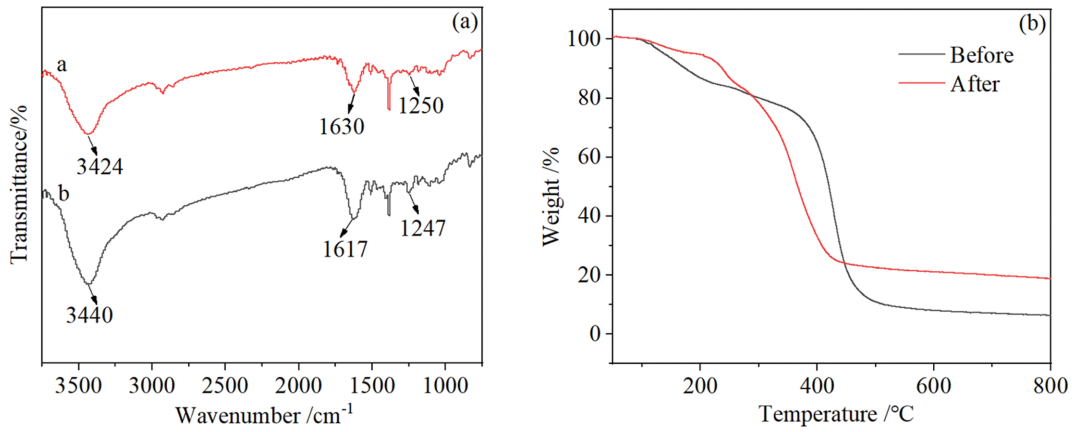

Fig. 2. (a) FT-IR spectra of the Cu(II)-IIP before (a) and after (b) adsorption for Cu(II) and (b) TGA curves of the Cu(II)-IIP before and after adsorption for Cu(II).

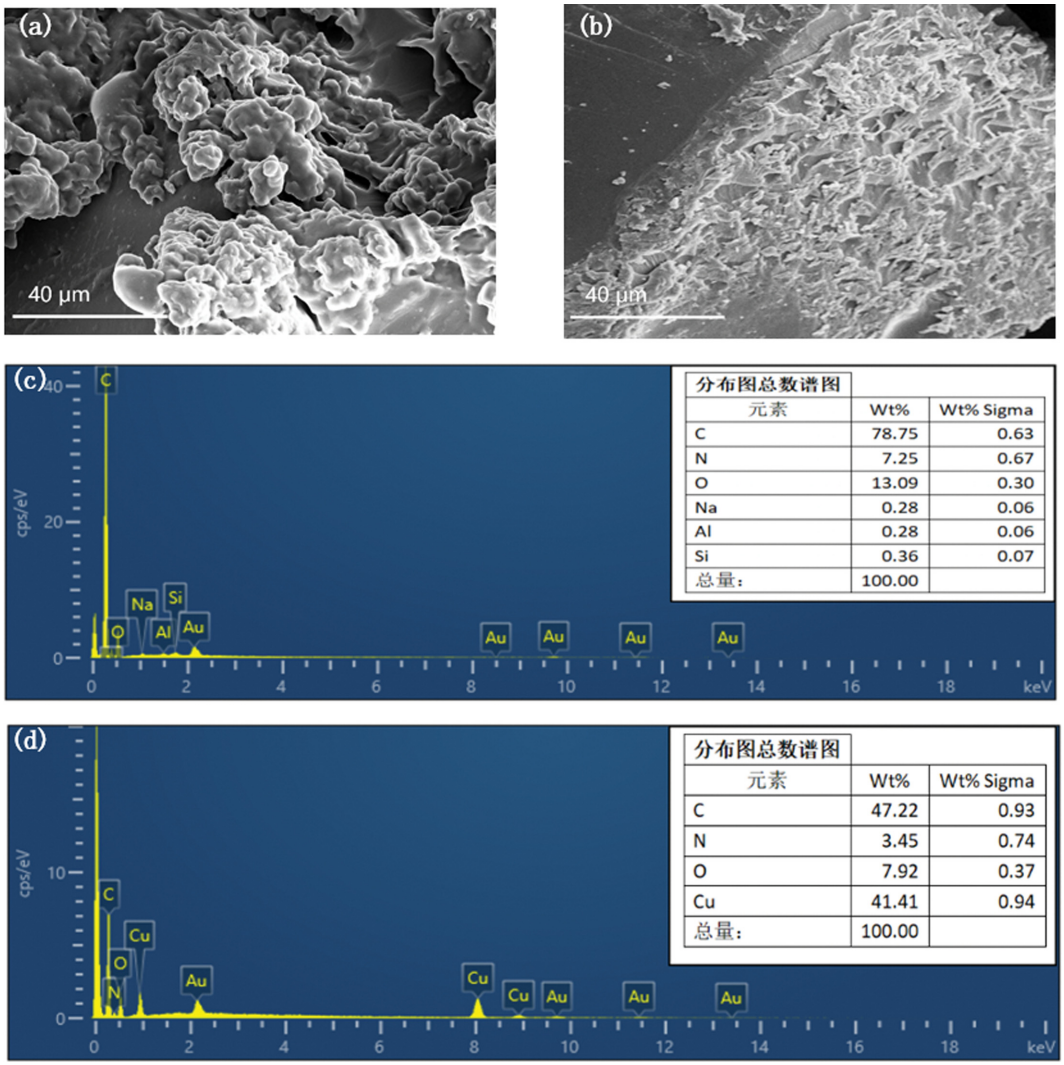

Fig. 3. The SEM images of the Cu(II)-IIP (a) before and (b) after adsorption for Cu(II), the EDS analysis diagram of the Cu(II)-IIP (c) before and (d) after adsorption for Cu(II).

and after the adsorption of Cu(II), respectively. The surface of Cu(II)-IIP before adsorption shows microspheres stacked, rough and porous, which provided a certain quantity of adsorption sites for the adsorption of Cu(II) due to a large number of imprinted cavities left by the elution of template ions [34]. This indicates the surface of Cu(II)-IIP was flatter after adsorption compared with that before adsorption, which was because a large number of imprinted cavities are occupied by Cu(II) during the adsorption process, so that Cu(II) ions have interacted with Cu(II)-IIP [35]. To further investigate the performance of Cu(II)-IIP, EDS analysis was performed on the samples before and after adsorption. From the EDS energy spectrum, compared with before adsorption (Fig. 3(c)), the Cu peak appears in the spectrum after adsorption (Fig. 3(d)) and the mass percentage of the Cu element also reaches 41.41 wt%, which indicates that Cu(II) was successfully adsorbed during the adsorption process [36]. Furthermore, the Brunauer-Emmett-Teller (BET) analysis studies were performed on the samples. Based on the experimental results, it was known that the surface area of Cu(II)-IIP was relatively small at 3.652 m^2/g and the total pore volume was 0.0054 cm^3/g (relevant data was not provided due to the small surface area).

2. The Influence of pH Value, Effect of the Initial Concentration of Metal Ions, Adsorption Kinetics Studies and Adsorption Isotherm of Cd(II) and Thermodynamic Analysis

The impact of pH on the equilibrium adsorption capacity is shown in Fig. 4(a). The adsorption impact of Cu(II)-IIP for Cu(II) does not differ significantly in the pH range of 3-6. The adsorption amounts for Cu(II) solutions with an initial concentration of 100 mg/L are all above 66 mg/g, and the best adsorption effect is achieved at pH=5.0. When the pH is low, the higher H^+ concentration may cause the formation of $-NH^{3+}$ on Cu(II)-IIP, thus reducing the chelation effect for Cu(II) ions, resulting in lower adsorption. When the pH gradually increases, the repulsion between protonation and metal ions gradually decreases and the adsorption amount increases. In summary, pH=5.0 was chosen for the subsequent adsorption experiments [37,38].

Fig. 4(b) shows the adsorption capacity and removal rates of Cu(II)-IIP and Cu(II)-NIP as the impacts of different initial Cu(II)

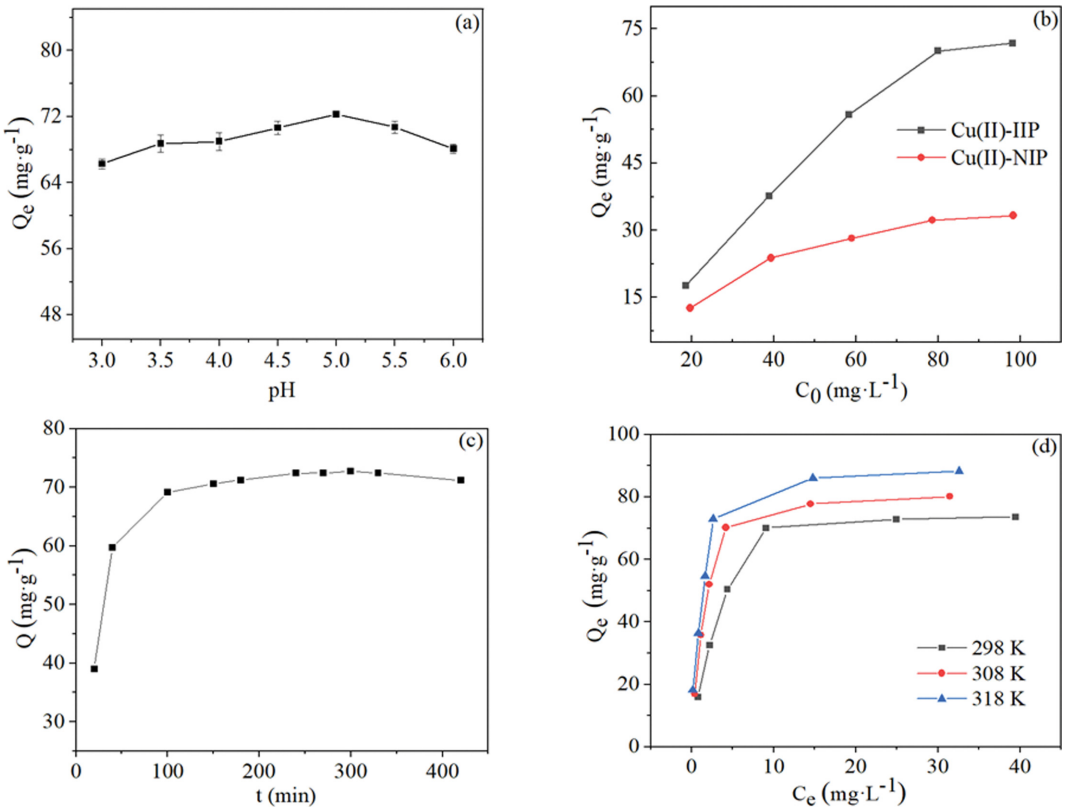

Fig. 4. (a) The influence of pH on the adsorption volume for Cu(II) ions (C_0=100 mg/L, T=298 K, t=12 h), (b) influence of the initial ion concentration on the adsorption for Cu(II) by Cu(II)-IIP and Cu(II)-NIP (pH=5.0, T=298 K), (c) influence of the adsorption time on the adsorption capacity of the Cu(II)-IIP material (pH=5.0, T=298 K, C_0=100 mg/L) and (d) influence of the different adsorption temperature on equilibrium adsorption of the Cu(II)-IIP (pH=5.0, t=5 h).

Table 1. Parameters of pseudo-first order and pseudo-second order kinetic models

Metal ion	Pseudo-first-order			Pseudo-second-order		
	K_1 (min^{-1})	Q_e ($mg·g^{-1}$)	R^2	K_2 ($g·mg^{-1}·min^{-1}$)	Q_e ($mg·g^{-1}$)	R^2
Cu(II)	1.10×10^{-2}	14.67	0.739	1.19×10^{-3}	75.19	0.999

concentrations. The adsorption amounts of Cu(II)-IIP and Cu(II)-NIP increase with an initial concentration of Cu(II), and the saturation adsorption amounts of Cu(II)-IIP and Cu(II)-NIP are 71.78 mg/g and 33.28 mg/g at the initial concentration of 100 mg/L. This is because Cu(II)-IIP has a large number of imprinted cavities compared to Cu(II)-NIP, the Cu(II) ions fill into imprinted cavities with increasing concentration, making the Cu(II)-IIP have a considerably higher adsorption capacity than Cu(II)-NIP [26,39]. Therefore, the initial concentration of 100 mg/L was chosen for subsequent experimental research.

In Fig. 4(c), the effect of adsorption time on the adsorption experiment is depicted. With the increase of time, a great quantity of imprinted sites on the surface of Cu(II)-IIP are filled rapidly and the adsorption rate accelerates rapidly, and the rate levels off at 100 min, reaching the maximum adsorption amount of 72.78 mg/g at 300 min.

To better understand the kinetics of Cu(II)-IIP for Cu(II) ions, the pseudo-first-order (Eq. (6)) and pseudo-second-order (Eq. (7)) kinetic models were used to elucidate [40]:

Pseudo-first-order kinetic model:

$$\ln(Q_e - Q_t) = \ln Q_e - K_1 t \quad (6)$$

Pseudo-second-order kinetic model:

$$\frac{t}{Q_t} = \frac{1}{K_2 Q_e^2} + \frac{t}{Q_e} \quad (7)$$

where K_1 represents the pseudo-first-order equation kinetic model rate constant, min^{-1}. K_2 represents the pseudo-second-order equation kinetic model rate constant, $g·(mg·min^{-1})$. Additionally, the parameters of the two kinetic models shown in Table 1 were derived from the relevant experimental data.

The individual parameters fitted to the kinetic model are listed in Table 1. The analysis of Fig. S1(a), (b) and Table 1 shows that the pseudo-second-order kinetic correlation coefficient (R^2=0.999) is closer to 1 than the pseudo-first-order kinetic correlation coefficient (R^2=0.739), indicating that the Cu(II)-IIP for Cu(II) adsorption process is mainly chemisorption [41].

The interaction between Cu(II)-IIP and Cu(II) ions at different equilibrium concentrations and temperatures was investigated by

Table 2. Langmuir and Freundlich models parameters

T (K)	Langmuir			Freundlich		
	Q_m·(mg·g^{-1})	K_L·(L·mg^{-1})	R^2	K_F·((mg·g^{-1}) (L·mg^{-1})$^{1/n}$)	n	R^2
298	79.11	0.4015	0.997	22.94	2.633	0.827
308	83.68	0.8031	0.999	32.07	2.956	0.784
318	91.58	1.1234	0.991	40.16	3.452	0.850

the adsorption isotherm system. According to Fig. 4(d), the adsorption capacity increases with increase of temperature and equilibrium concentration of Cu(II), indicating that the temperature increase at 298, 308 and 318 K is more favorable for adsorption of Cu(II) ions by Cu(II)-IIP. For investigating more clearly the adsorption behavior of Cu(II) by Cu(II)-IIP, data in Fig. 4(d) were fitted using Langmuir and Freundlich isotherm models. The Langmuir isotherm model usually involves monolayer adsorption and the Freundlich isotherm model the multilayer adsorption. To better understand the adsorption behavior, the Langmuir isotherm model (Eq. (8)) and Freundlich isotherm model (Eq. (9)) were used to elucidate [42,43]:

Langmuir isotherm model:

$$\frac{C_e}{Q_e}=\frac{C_e}{Q_m}+\frac{1}{K_L Q_m} \tag{8}$$

Freundlich isotherm model:

$$\ln Q_e=\ln K_F+\frac{1}{n}\ln C_e \tag{9}$$

where Q_m (mg·g^{-1}) denotes the saturation adsorption amount, K_L (L·mg^{-1}) represents the adsorption equilibrium constant, K_F ((mg·g^{-1}) (L·mg^{-1})$^{1/n}$) represents the Freundlich constant, which are connected to adsorption capacity and strength, respectively.

Fig. S2(a) and Fig. S2(b) show the plots of Langmuir and Freundlich isotherm models and Table 2 displays the specific results of the fitting; the fitted correlation coefficients of the Langmuir model are both close to 1, while the correlation fitting coefficients of the Freundlich model are both lower than those of the Langmuir model [44]. Therefore, the Langmuir model is better consistent with Cu(II)-IIP to the adsorption behavior of Cu(II). Similar findings were reported for different pollutant and other adsorbent systems in literature [45,46]. And by comparing the data in the table, it can be concluded that the theoretical maximum adsorption capacity of Cu(II)-IIP reaches 91.58 mg/g when adsorption temperature is at 318 K.

To further investigate the thermodynamic parameters and reaction mechanism, the adsorption thermodynamics of Cu(II)-IIP for Cu(II) was studied at 298, 308 and 318 K. The thermodynamic parameters Gibb's free energy change ΔG^0 (kJ/mol), enthalpy change ΔH^0 (kJ/mol), and entropy change ΔS^0 (J/(mol·K) were found by Eqs. (10), (11), and (12) [36,47].

$$K^0=\frac{Q_e}{C_e} \tag{10}$$

$$\ln K^0=-\frac{\Delta H^0}{RT}+\frac{\Delta S^0}{R} \tag{11}$$

Table 3. Thermodynamic parameters of Cu(II)-IIP adsorption for Cu(II)

T (K)	lnK^0	ΔG^0 (kJ/mol)	ΔH^0 (kJ/mol)	ΔS^0 (J/(mol·K))
298	0.165	−0.41		
308	0.410	−1.05	30.11	87.79
318	0.822	−2.17		

$$\Delta G^0=\Delta H^0-T\Delta S^0 \tag{12}$$

where R (8.314 J·mol^{-1}·K^{-1}) is the gas constant, T (K) is the absolute temperature in Kelvin. The thermodynamic parameters calculated from the above expressions are shown in Table 3.

As demonstrated by Table 3, $\Delta G^0<0$ and $\Delta H^0>0$ show the adsorption of Cu(II) is a spontaneous heat absorption reaction, and the temperature increase in the range of 298-318 K can effectively promote the adsorption of Cu(II)-IIP on Cu(II). Meanwhile, $\Delta S^0>0$ indicates that this is an entropy-increasing adsorption process [48]. According to the description in the relevant literature, the value of ΔH^0 is between 20.9 and 418.4 kJ/mol. This adsorption process is chemisorption, which indicates that the charge is shared or transferred from the adsorbent surface to the adsorbed ions, thus forming a coordination bond [47]. Therefore, the ΔH^0 value of 30.11 kJ/mol for this adsorption process, which indicates the adsorption of Cu(II) on Cu(II)-IIP is chemisorption.

3. Selectivity Analysis

To learn more about the adsorption selectivity of Cu(II)-IIP and Cu(II)-NIP, competitive adsorption was performed from mixed solutions of heavy metal ions containing (Cd(II), Mn(II), Zn(II),

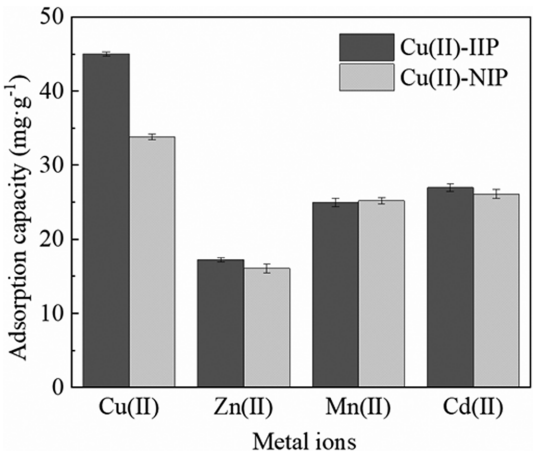

Fig. 5. The selectivity adsorption properties of the Cu(II)-IIP and Cu(II)-NIP for Cu(II) ions (C_0=100 mg/L, pH=5.0, T=298 K, t=5 h, n=3).

Table 4. The selectivity parameters of Cu(II)-IIP and Cu(II)-NIP

Element	$Q_{eCu(II)\text{-}IIP}$ ($mg \cdot g^{-1}$)	$Q_{eCu(II)\text{-}NIP}$ ($mg \cdot g^{-1}$)	α	β
Cu(II)	45.04	33.88	1.32	-
Zn(II)	17.28	16.10	1.07	1.23
Mn(II)	25.03	25.24	0.99	1.33
Cd(II)	27.02	26.16	1.03	1.28

Cu(II)) [49]. The selective adsorption data of Cu(II)-IIP and Cu(II)-NIP on Cu(II) are shown in Fig. 5 and Table 4. The adsorption amounts of Cu(II)-IIP and Cu(II)-NIP on Cu(II) in mixed solutions are higher than those of Zn(II), Mn(II), and Cd(II), while the Cu(II)-IIP adsorption amount is greater than Cu(II)-NIP adsorption amount. Meanwhile, the β values are in the range of 1.23-1.33, reflecting that the adsorption of Cu(II)-IIP on Cu(II) is greater than its adsorption on competing ions, and Cu(II)-IIP has a better selectivity for Cu(II) [50]. It was concluded that the high adsorption of Cu(II)-IIP on Cu(II) was attributed to the fact that Cu(II)-IIP has imprinted vacancies and binding sites matching Cu(II) ions.

4. Reusability Studies

Adsorbent regeneration is the primary determinant of its ability to recycle. It can only be effectively reused if it has strong adsorption and desorption capabilities [51]. As seen by Fig. 6, the removal rate decreases partially during the adsorption-desorption cycle, which may be because some Cu(II) is not successfully eluted on the adsorption site during the desorption process. The removal rate of the Cu(II)-IIP remains above 85% after five adsorption cycles, it is evident that the Cu(II)-IIP performs well during cycling, good adsorption stability and reuse performance. Table 5 provides the maximum adsorption capacities of certain adsorbent materials reported in recent years for Cu(II) ions. Additionally, it is concluded that compared to Cu(II) imprinted materials prepared from other raw materials, the Cu(II)-IIP has a better adsorption capability for Cu(II) adsorption. Therefore, Cu(II)-IIP is a better choice in the selection of adsorbents for treating aqueous solutions containing Cu(II) ions.

5. Adsorption Mechanism

5-1. XPS Analysis

Based on the above experimental work, the X-ray photoelectron spectroscopy before and after the adsorption of Cu(II)-IIP was further analyzed as shown in Fig. 7. Among them, Fig. 7(a) shows the full spectrum of Cu(II)-IIP before and after adsorption, and the newly appeared Cu2p3 characteristic peak after adsorption verifies the successful combination of Cu(II)-IIP and Cu(II) [44]. As can be seen from Fig. 7(b), the O1s spectrum consists of two fitted peaks of the O-H band and the O-C band. By comparing O-H (531.08 eV) and O-C (532.51 eV) before adsorption and O-H (531.40 eV) and O-C (532.39 eV) after adsorption, these show the O-H peak and O-C peak have been shifted to a smaller extent, indicating that the hydroxyl group might have been chelated with Cu(II) (532.39 eV); the O-H peak and O-C peak show a small shift, indicating that the hydroxyl group might have been weakly chelated with Cu(II) occurred relatively weak chelation [55]. Fig. 7(c) shows the N1s spectrum before and after the adsorption of Cu(II)-IIP. The N1s spectrum before the adsorption consists of two fitted peaks of N-H (399.03 eV) and $-NH_2$ (400.74 eV), and the N-H and $-NH_2$ peaks are shifted to 399.68 and 401.54 eV after the adsorption, indicating the involvement of N-H or $-NH_2$ in this process, while it is consistent with the FT-IR analysis of the results [44]. Moreover, the -N-Cu peak formed by ion exchange appears at 406.46 eV, indicating strong chelation of amino groups with Cu(II) during the adsorption process.

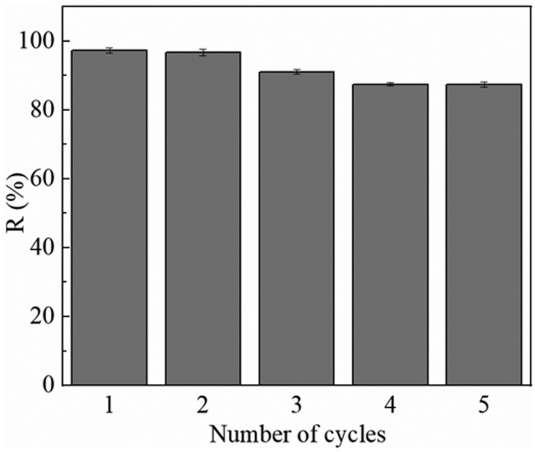

Fig. 6. Five adsorption-desorption cycles of the Cu(II)-IIP for Cu(II) ions (C_0=40 mg/L, pH=5.0, T=298 K, t=5 h).

XPS and FT-IR studies indicate that the interaction of Cu(II) with O and N atom related functional groups on Cu(II)-IIP may occur in the form of -O-Cu and -N-Cu.

CONCLUSIONS

We prepared Cu(II)-IIP and evaluated the adsorption efficiency of Cu(II) on Cu(II)-IIP. From the static adsorption experimental

Table 5. Comparison of the different Cu(II)-imprinted polymers

Adsorbent	$Q_m \cdot (mg \cdot g^{-1})$	pH	T (K)	Refs.
Cu(II) ion-imprinted polymer	39.82	6.0	298	[38]
IIP/Mt/Cu	23.60	5.0	298	[52]
Cu-IIM	48.00	6.0	298	[18]
Cu-IIP	83.33	5.7	298	[53]
(Cu-PEI)-imprinted hydrogel	40.00	5.5	330	[54]
Cu(II)-IIP	91.58	5.0	318	this work

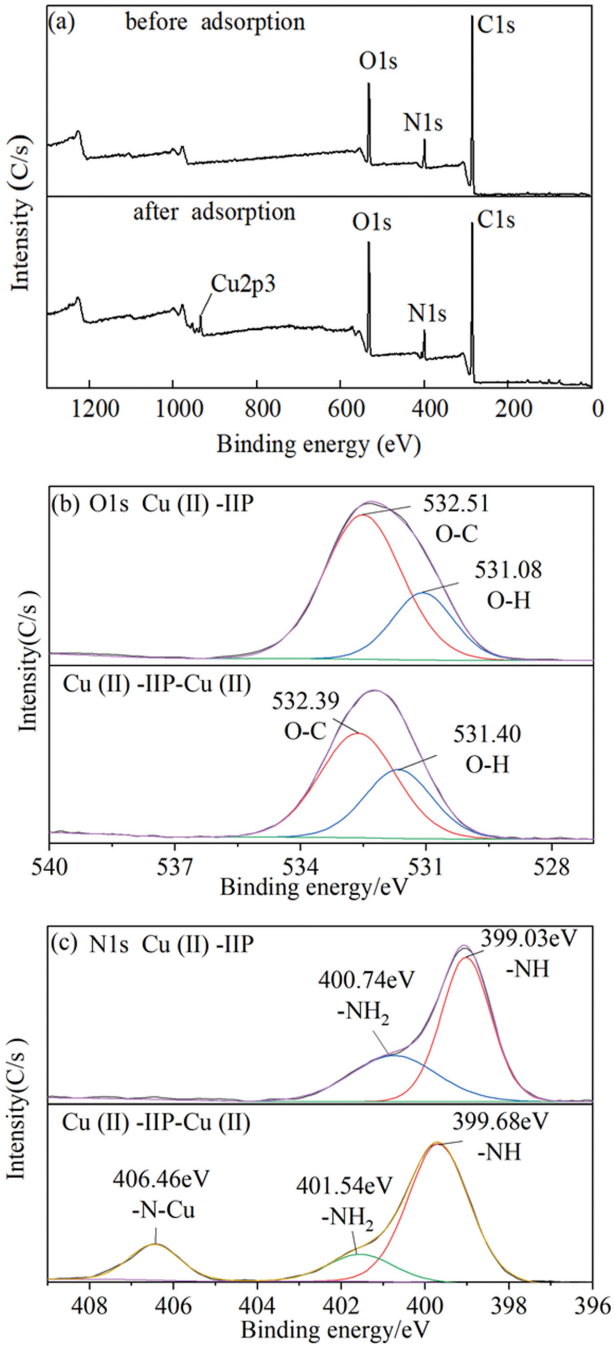

Fig. 7. (a) The full XPS spectrum before and after the Cu(II) ions adsorption, (b) O 1s and (c) N 1s narrow XPS scan before and after the Cu(II) ions adsorption.

study, Cu(II)-IIP reached the maximum adsorption capacity of 91.58 mg/g at pH=5 and T=318 K. The isotherm study and kinetic study reveals that the adsorption isotherm is in accordance with the Langmuir model, and is dominated by monolayer adsorption; the adsorption kinetics satisfies the pseudo-second-order kinetic equation and mainly exhibits chemisorption; the adsorption thermodynamic study shows that the adsorption of Cu(II)-IIP on Cu(II) is a spontaneous heat absorption reaction. Cu(II)-IIP showed good selective adsorption of Cu(II) in aqueous solutions where multiple competing ions coexisted. Cu(II)-IIP showed better adsorption than NIP. The removal rate was above 85% after five reusable experiments. Meanwhile, the morphological characteristics of Cu(II)-IIP before and after the adsorption of Cu(II), as well as the EDS energy spectrum observed by SEM, indicated that Cu(II)-IIP had a certain adsorption capacity for Cu(II). In addition, the mechanism of adsorption was investigated by XPS and FT-IR, and the synergistic complexation of N and O groups in the adsorption process was suggested. In conclusion, the Cu(II)-IIP offers a broad prospects for Cu(II) removal from the aqueous environment.

ACKNOWLEDGEMENTS

This work was supported by the Natural Science Foundation of Hunan Province (2020JJ4509), Key Projects of the Education Department of Hunan Province (21A0345), Key Laboratory of Mineral Cleaner Production and Exploit of Green Functional Materials in Hunan Province, P. R. China.

DECLARATIONS

All the authors declare that they have no known competing financial interests or personal relationships that could have appeared to influence the work reported in this paper.

SUPPORTING INFORMATION

Additional information as noted in the text. This information is available via the Internet at http://www.springer.com/chemistry/journal/11814.

REFERENCES

1. Q. Wang, S. Zhu, C. Xi and F. Zhang, *Front. Chem.*, **10**, 814643 (2022).
2. H. Li, D. Yao, Q. Feng, H. Zeng, J. Liang, Z. Zhou, Y. Tian, N. Zhou and X. Lu, *Desalin. Water Treat.*, **118**, 195 (2018).
3. S. Zhu, C. Xi, Y. Zhang and F. Zhang, *ACS Appl. Polym. Mater.*, **4**, 9284 (2022).
4. S. He, F. Zhang, S. Cheng and W. Wang, *ACS Sustain. Chem. Eng.*, **4**, 3948 (2016).
5. N. Zhou, H. Chen, Q. Feng, D. Yao, H. Chen, H. Wang, Z. Zhou, H. Li, Y. Tian and X. Lu, *J. Clean. Prod.*, **165**, 221 (2017).
6. P. Zhou, H. Yuan, L. Ou and Z. Peng, *J. Macromol. Sci. A*, **56**, 717 (2019).
7. J. Ma, Y. Xiong, X. Dai and F. Yu, *Chem. Eng. J.*, **380**, 122387 (2020).
8. K. W. Jung, S. Y. Lee, J. W. Choi and Y. J. Lee, *Chem. Eng. J.*, **369**, 529 (2019).
9. G. Stando, P. M. Hannula, B. Kumanek, M. Lundström and D. Janas, *Water Resour. Ind.*, **26**, 100156 (2021).
10. Z. Yang, T. Hou, J. Ma, B. Yuan, Z. Tian, W. Yang and N. J. Graham, *Water Res.*, **177**, 115775 (2020).
11. Y. Li, C. Liu, P. Xu, M. Li, M. Zen and S. Tang, *Chem. Eng. J.*, **243**, 108 (2014).
12. K. Chen and W. Zeng, *Polymers*, **13**, 962 (2021).
13. H. Cao, P. Yang, T. Ye, M. Yuan, J. Yu, X. Wu, F. Yin, Y. Li and F.

Xu, *Chemosphere*, **278**, 130369 (2021).
14. L. Qin, Y. Zhao, L. Wang, L. Zhang, S. Kang, W. Wang, T. Zhang and S. Song, *Chemosphere*, **252**, 126560 (2020).
15. G. Sharma and B. Kandasubramanian, *J. Chem. Eng. Data*, **65**, 396 (2020).
16. F. Shafizadeh, M. Taghizadeh and S. Hassanpour, *Environ. Sci. Pollut. Res.*, **26**, 18493 (2019).
17. J. Shah and M. R. Jan, *J. Anal. Chem.*, **73**, 1146 (2018).
18. Z. Wang, D. Kong, N. Qiao, N. Wang, Q. Wang, H. Liu, Z. Zhou and Z. Ren, *Appl. Surf. Sci.*, **457**, 981 (2018).
19. B. Ara, M. Muhammad, Z. Rani, T. U. H. Zia and K. Gul, *Desalin. Water Treat.*, **191**, 173 (2020).
20. M. Monier, I. Youssef and A. El-Mekabaty, *Polym. Int.*, **69**, 31 (2020).
21. P. Wei, Z. Li, X. Zhao, R. Song and Z. Zhu, *J. Taiwan Inst. Chem. E.*, **113**, 107 (2020).
22. S. Wang and R. Zhang, *Sep. Sci. Technol.*, **42**, 1079 (2007).
23. S. Wang and S. Wang, *J. AOAC Int.*, **99**, 279 (2016).
24. S. Wang and R. Zhang, *Anal. Chim. Acta.*, **575**, 166 (2006).
25. Z. Bahadır, G. Kültür, M. Yazar, D. Çakır and C. Duran, *Anal. Lett.*, **55**, 1847 (2022).
26. Q. Wang, S. Zhu, C. Xi, Y. Shen, Y. Xiang and F. Zhang, *J. Appl. Polym. Sci.*, **139**, 51866 (2021).
27. Z. Zhou, Z. Xu, Q. Feng, D. Yao, J. Yu, D. Wang, S. Lv, Y. Liu, N. Zhou and M. Zhong, *J. Clean. Prod.*, **187**, 996 (2018).
28. S. Rais, A. Islam, I. Ahmad, S. Kumar, A. Chauhan and H. Javed, *Food Chem.*, **334**, 127563 (2020).
29. X. Huang, J. Song, H. Li, M. Gong and Y. Zhang, *J. Hazard. Mater.*, **365**, 53 (2019).
30. J. W. Yu, J. Jung, Y. M. Choi, J. H. Choi, J. Yu, J. K. Lee, N. H. You and M. Goh, *Polym. Chem.*, **7**, 36 (2016).
31. L. Zhu, R. Hu, Y. Xiang, X. Yang, Z. Chen, L. Xiong, X. Wu, Z. He and W. Lei, *Int. J. Energy Res.*, **45**, 6002 (2021).
32. M. Monier, A. A. H. Bukhari and N. H. Elsayed, *Int. J. Biol. Macromol.*, **155**, 795 (2020).
33. H. Liu, D. Kong, W. Sun, Q. Li, Z. Zhou and Z. Ren, *Chem. Eng. J.*, **303**, 348 (2016).
34. P. Wei, Z. Zhu, R. Song, Z. Li and C. Chen, *Electrochim. Acta*, **317**, 93 (2019).
35. J. Fei, X. Wu, Y. Sun, L. Zhao, H. Min, X. Cui, Y. Chen, S. Liu, H. Lian and C. Li, *Anal. Chim. Acta*, **1162**, 338477 (2021).
36. Q. Wang, S. Zhu, C. Xi, B. Jiang and F. Zhang, *ACS Omega*, **7**, 12231 (2022).
37. K. Suzuki, T. Kato, S. Fuchida and C. Tokoro, *Chem. Geol.*, **550**, 119744 (2020).
38. Z. Ren, X. Zhu, J. Du, D. Kong, N. Wang, Z. Wang, Q. Wang, W. Liu, Q. Li and Z. Zhou, *Appl. Surf. Sci.*, **435**, 574 (2018).
39. Q. Huang, M. Liu, J. Zhao, J. Chen, G. Zeng, H. Huang, J. Tian, Y. Wen, X. Zhang and Y. Wei, *Appl. Surf. Sci.*, **427**, 535 (2018).
40. Z. Cheng, J. Liao, B. He, F. Zhang, F. Zhang, X. Huang and L. Zhou, *ACS Sustain. Chem. Eng.*, **3**, 1677 (2015).
41. A. Islam and A. Chauhan, *Environ. Sci. Pollut. Res.*, **29**, 69068 (2022).
42. H. Liu, Q. Wang and F. Zhang, *ACS Omega*, **5**, 8816 (2020).
43. H. Tian, L. Mao, K. Li and H. Li, *Sep. Sci. Technol.*, **56**, 3136 (2021).
44. Y. He, P. Wu, W. Xiao, G. Li, J. Yi, Y. He, C. Chen, P. Ding and Y. Duan, *PLoS One*, **14**, e0213377 (2019).
45. O. Duman, T. G. Polat, C. O. Diker and S. Tunc, *Int. J. Biol. Macromol.*, **160**, 823 (2020).
46. O. Duman, T. G. Polat and S. Tunc, *J. Environ. Manage.*, **322**, 116130 (2022).
47. H. Liu, F. Zhang and Z. Peng, *Sci. Rep.*, **9**, 3663 (2019).
48. Y. Pang, C. Zhao, Y. Li, Q. Li, X. Bayongzhong, D. Peng and T. Huang, *Sci. Rep.*, **12**, 4424 (2022).
49. M. V. Dinu, I. A. Dinu, M. M. Lazar and E. S. Dragan, *Carbohydr. Polym.*, **186**, 140 (2018).
50. N. H. Elsayed, M. Monier and R. A. S. Alatawi, *Mater. Chem. Phys.*, **264**, 124433 (2021).
51. Y. Dai, L. Zhou, X. Tang, J. Xi, J. Ouyang, Z. Liu, G. Huang and A. Adesina, *Int. J. Biol. Macromol.*, **164**, 4155 (2020).
52. R. Msaadi, G. Yilmaz, A. Allushi, S. Hamadi, S. Ammar, M. M. Chehimi and Y. Yagci, *Polymers*, **11**, 286 (2019).
53. W. Zhang, M. Yun, Z. Yu, D. Chen and X. Li, *Polym. Bull.*, **76**, 1861 (2018).
54. J. Wang and Z. Li, *J. Hazard. Mater.*, **300**, 18 (2015).
55. H. Cao, P. Yang, T. Ye, M. Yuan, J. Yu, X. Wu, F. Yin, Y. Li and F. Xu, *Chemosphere*, **278**, 130369 (2021).

Supporting Information

Synthesis and characterization of epoxy resin-based ion-imprinted polymer for selective removal of copper ions

Sining Zhu, Haitao Wan, Zhibo Yan, Chen Xi, Yuzhuo Zhang, and Fan Zhang†

College of Chemistry and Chemical Engineering, National Experimental Teaching Demonstration Center for Chemistry, Jishou University, Jishou 416000, China

(*Received 28 November 2022 • Revised 3 April 2023 • Accepted 7 April 2023*)

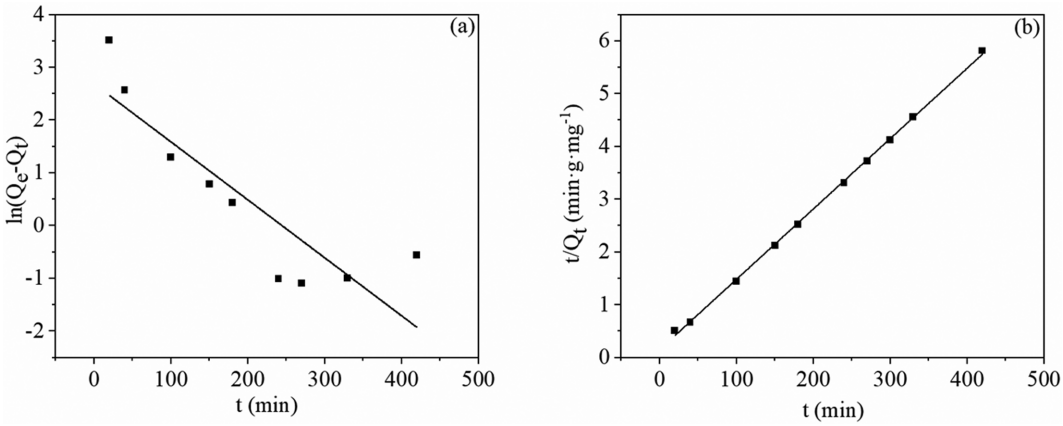

Fig. S1. (a) The quasi-first-order model fitting curve and (b) the quasi-second-order model fitting curve from the influence of time on the adsorption effect of the Cu(II)-IIP material (pH=5.0, T=298 K, C_0=100 mg/L).

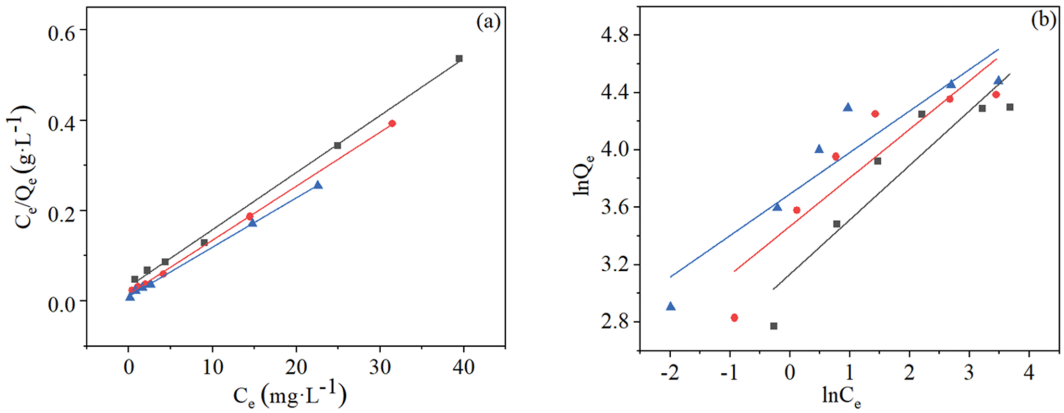

Fig. S2. (a) The Langmuir model and (b) the Freundlich model from the adsorption isotherms of Cu(II) adsorption on the Cu(II)-IIP and Cu(II)-NIP (pH=5.0, t=5 h).